ADVANCED NANOBIOMED RESEARCH Open Access
www.advnanobiomedres.com

Pyrolyzed Walnut Shell-Based Flexible Electrodes for Magnetically Triggered ON/OFF DNA Release

Paolo Bollella, Blanca Cassano, Verdiana Marchianò, Angelo Tricase, Eleonora Macchia, and Luisa Torsi**

A magnetically gated, enzymatically driven DNA release platform based on sustainable pyrolyzed walnut shell-derived carbon electrodes is reported. Upon glucose addition under aerobic conditions, biocatalytic oxygen reduction at the cathode induces a local pH increase, resulting in electrostatic repulsion of negatively charged 5(6)-carboxyfluorescein-labeled DNA (FAM-labeled DNA). Electrochemical analysis reveals an oxygen reduction reaction (ORR) onset potential of $+0.576 \pm 0.003$ V vs. Ag/AgCl and a maximum current of -8.2 ± 0.4 µA. Electrochemical impedance spectroscopy (EIS) confirms a post-ORR increase in interfacial resistance from 6.2 ± 0.5 to 11.1 ± 0.9 kΩ. DNA release reaches 97% after 400 min, corresponding to a surface density of 22 ± 4 nmol cm^{-2}. A competing enzymatic gate, composed of co-immobilized glucose oxidase and catalase (GOx–CAT) on magnetic nanoparticles (MNPs), enables remote suppression of electron flow and DNA release upon application of a 0.3 T magnetic field. Under "OFF" conditions, DNA release is reduced to 1%, and anodic current decreases by 60%. The system exhibits excellent reversibility over four ON–OFF cycles with minimal performance degradation. This bioelectronic platform represents a self-powered, reversible strategy for stimuli-responsive drug release.

1. Introduction

The ability to trigger the release of biomolecules in response to specific external stimuli is a key concept underpinning the design of advanced bioelectronic, biomedical, and biotechnological systems.[1,2] This spatiotemporally controlled release is central to applications such as targeted drug delivery, biosensing, molecular computing, and the dynamic assembly of nanostructured systems.[3–5] Among functional biomolecular components, DNA has emerged as a particularly powerful material due to its predictable base-pairing, structural rigidity, and high programmability—enabling its integration into diverse tasks spanning information processing to interface engineering.[6,7] To enable stimuli-responsive DNA release, various external triggers—including light, temperature variations, mechanical inputs, and electromagnetic fields—have been successfully employed.[8–12] Among these, electrochemical activation offers distinct advantages, such as high spatial resolution, real-time tunability, and the use of compact, low-power instrumentation.[13–15] However, many conventional electrochemical systems rely on irreversible reactions, including the degradation of functional polymers or the cleavage of covalent bonds, which restrict their reusability and operational longevity.[16–18] Reversible release mechanisms based on noncovalent interactions, such as boronic acid–diol chemistry, provide a milder and reusable alternative, yet they often demand narrow potential windows or elevated voltages, which can pose limitations in biologically relevant conditions.[19,20]

Alongside the evolution of functional bioelectronic interfaces, there is growing emphasis on the development of self-sustaining and environmentally responsible platforms.[21,22] Recent innovations in self-powered biosensors and integrated therapeutic devices—capable of autonomously detecting, processing, and responding to biological signals—have opened new directions in precision medicine and decentralized diagnostics.[23] These

P. Bollella, B. Cassano, L. Torsi
Department of Chemistry
University of Bari A. Moro
Via E. Orabona 4, 70125 Bari, Italy
E-mail: paolo.bollella@uniba.it; luisa.torsi@uniba.it

The ORCID identification number(s) for the author(s) of this article can be found under https://doi.org/10.1002/anbr.202500131.

DOI: 10.1002/anbr.202500131

P. Bollella, V. Marchianò, A. Tricase, E. Macchia, L. Torsi
Centre for Colloid and Surface Science
University of Bari A. Moro
Via E. Orabona 4, 70125 Bari, Italy

V. Marchianò, A. Tricase, E. Macchia
Department of Pharmacy-Pharmaceutical Science
University of Bari A. Moro
Via E. Orabona 4, 70125 Bari, Italy

E. Macchia
Faculty of Science and Engineering
Åbo Akademi University
20500 Turku, Finland

systems often utilize biofuel-driven enzymatic reactions to generate electrical energy in situ, allowing for autonomous operation without the need for external power.[24,25] Concurrently, increasing environmental concerns have prompted the integration of biodegradable, nontoxic, and resource-efficient materials into bioelectronic architectures, promoting the transition toward greener technologies.[26]

Within this framework, carbon materials derived from renewable biomass have emerged as attractive alternatives to conventional electrode materials. In this study, we focus on the fabrication of carbon electrodes through the pyrolysis of walnut shells, a commonly available agricultural byproduct. This approach exemplifies sustainable material engineering by transforming waste lignocellulosic biomass into high-performance carbon materials via an energy-efficient and scalable thermal process. Due to their inherent hardness, high carbon yield, and porous structure, walnut shells serve as an ideal precursor for electroactive carbon synthesis. The resulting pyrolyzed material exhibits favorable properties such as high surface area, electrical conductivity, and surface chemical tunability, all of which are essential for robust electrochemical performance and biomolecular interfacing. These features, combined with the low environmental impact and cost-effectiveness of the starting material, make walnut shell-derived carbon electrodes highly suitable for integration into next-generation, sustainable bioelectronic devices.

In this study, we present a magnetically switchable, dual-mode bioelectronic platform built on walnut shell-derived carbon electrodes. The bioanode is functionalized with pyrroloquinoline quinone-dependent glucose dehydrogenase (PQQ-GDH), immobilized via a polydopamine (PDA) adhesive layer, enabling efficient bioelectrocatalytic oxidation of glucose. The biocathode integrates laccase with silica nanoparticles co-functionalized with trigonelline and 4-carboxyphenylboronic acid (in a 1:4 molar ratio), forming a pH-sensitive electrostatic switching interface. This architecture is designed to trigger the release of 5(6)-carboxyfluorescein-labeled DNA (FAM-labeled DNA) upon oxygen reduction, which consumes local protons and induces a pH increase, defining the "ON" release state.

To achieve reversible gating, we incorporated a competing enzymatic module composed of glucose oxidase (GOx) and catalase (CAT) co-immobilized on magnetic nanoparticles (MNPs).[27] Upon application of an external magnetic field, these particles are drawn near the anode electrode, effectively outcompeting the PQQ-GDH-based anode for glucose and suppressing its catalytic activity. This enzymatic diversion inhibits proton consumption at the cathode, preventing the local pH shift necessary for DNA release (**Figure 1**).[28–30] This magnetically gated enzymatic control provides a robust framework for programmable bioelectronic systems in which biochemical substrates and physical stimuli can be integrated as logical inputs. The platform offers new possibilities for the development of dynamic biosensors, molecular logic gates, and closed-loop drug delivery devices.

2. Results and Discussion

To investigate magnetically regulated, electrochemically driven DNA release at sustainable carbon-based interfaces, we

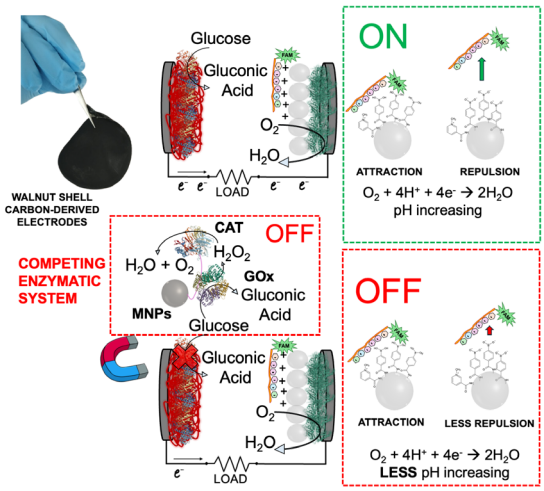

Figure 1. Scheme of sense-act-treat device based on walnut shell carbon-derived flexible electrode further modified with pyrroloquinoline quinone-dependent glucose dehydrogenase (PQQ-GDH) immobilized via PDA at the anode and laccase/SiO_2 (trigonelline:4-carboxyboronic acid 1:4 molar ratio) to load FAM-DNA. This is released upon ORR increasing pH locally. The process is deactivated with an enzymatic competition system based on glucose oxidase (GOx) and catalase co-immobilized onto MNPs and activated through an external magnetic field.

engineered a dual-functional sensing–actuating platform using pyrolyzed walnut shell-derived carbon electrodes.[31] These electrodes were independently functionalized at their anodic and cathodic domains to generate distinct bioelectronic functionalities. At the cathode, bilirubin oxidase (BOx) was integrated with silica nanoparticles co-functionalized with trigonelline and 4-carboxyphenylboronic acid (1:4 molar ratio), forming an electrostatically switchable surface capable of reversibly adsorbing 5(6)-carboxyfluorescein-labeled DNA (FAM–DNA). At the anode, pyrroloquinoline quinone-dependent glucose dehydrogenase (PQQ–GDH) was immobilized via an in situ polymerized PDA matrix, enabling bioelectrocatalytic glucose oxidation and sustained electron flow. This configuration allowed for localized pH modulation at the cathode via oxygen reduction, which induced a surface charge transition sufficient to trigger DNA desorption.

Cyclic voltammetry (CV) performed at the BOx/Tr^+–BA–SiO_2-functionalized cathode under aerobic conditions revealed a catalytic onset for the oxygen reduction reaction (ORR) at $+0.576 \pm 0.003$ V vs. Ag/AgCl, with a maximum catalytic current (ΔI_{cat}) of -8.2 ± 0.4 µA at 0 V (**Figure 2**A). The electrochemical signal was abolished under nitrogen-saturated conditions, confirming oxygen as the sole terminal electron acceptor. This catalytic activity was attributed to direct electron transfer (DET) mediated by the multicopper redox centers of BOx, in agreement with prior literature. Importantly, the system supports efficient electrocatalysis near 0 V vs. Ag/AgCl, representing a substantial decrease in overpotential compared to unmodified ITO or conventional carbon-based electrodes, which typically require potentials as negative as -0.5–-0.8 V.[28] This reduction in driving potential offers advantages for compatibility with physiological systems and minimizes interference from nonspecific redox processes.

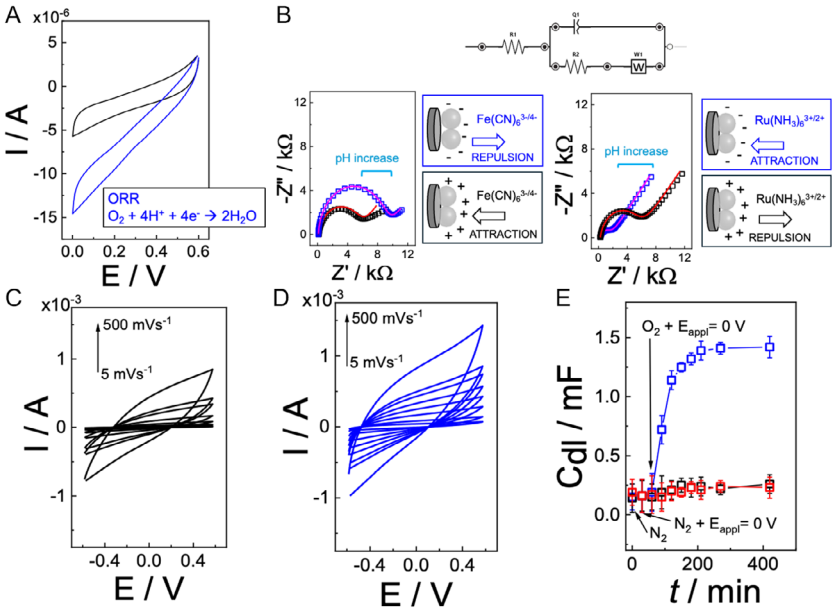

Figure 2. A) CVs for FAM-DNA/Tr^+-BA^-(1:4)-SiO_2/BOx/C electrode in 3 mM HEPES buffer pH 7 + 100 mM Na_2SO_4 under N_2 purging (black curve) and in open air (blue curve) at 5 mV s^{-1}. B) EIS curve performed in 5 mM $Fe(CN)_6^{3-/4-}$ (3 mM HEPES buffer pH 7 + 100 mM Na_2SO_4) before (black dots, no local pH change) and after applying 0 V vs. Ag/AgCl for 30 min in open air (blue dots, local pH change recharging the surface) and EIS curve performed in 5 mM $Ru(NH_3)_6^{3+/2+}$ (3 mM HEPES buffer pH 7 + 100 mM Na_2SO_4) before (black dots, no local pH change) and after applying 0 V vs. Ag/AgCl for 30 min in open air (blue dots, local pH change recharging the surface); *inset:* EIS equivalent Randles circuit to fit the data (red curve corresponding to black dots, magenta curve corresponding to blue dots). C) CVs for FAM-DNA/Tr^+-BA^-(1:4)-SiO_2/BOx/C electrode in 3 mM HEPES buffer pH 7 + 100 mM Na_2SO_4 at different scan rates (5–500 mV s^{-1}) after the application of 0 V vs. Ag/AgCl for 30 min under N_2 purging. D) CVs for FAM-DNA/Tr^+-BA^-(1:4)-SiO_2/BOx/C electrode in 3 mM HEPES buffer pH 7 + 100 mM Na_2SO_4 at different scan rates (5–500 mV s^{-1}) after the application of 0 V vs. Ag/AgCl for 30 min in open air for ORR. E) Double-layer capacitance variation under ORR at 0 V vs. Ag/AgCl in 3 mM HEPES buffer pH 7 + 100 mM Na_2SO_4: FAM-DNA/Tr^+-BA^-(1:4)-SiO_2/BOx/C electrode (blue curve), FAM-DNA/Tr^+-BA^-(1:4)-SiO_2/C electrode (black curve, control experiment) and FAM-DNA/Tr^+-SiO_2/BOx/C electrode (red curve, control experiment).

To characterize interfacial properties, electrochemical impedance spectroscopy (EIS) was conducted using $[Fe(CN)_6]^{3-/4-}$ as the redox probe. After 30 min of ORR at 0 V under aerobic conditions, the charge transfer resistance (R_{CT}) of the BOx/Tr^+–BA–SiO_2/C interface increased markedly from 6.2 ± 0.5 to 11.1 ± 0.9 kΩ (Figure 2B, measured in $Fe(CN)_6^{3-/4-}$) and decreased from 5.4 ± 0.1 to 1.5 ± 0.1 kΩ (Figure 2B, measured in $Ru(NH_3)_6^{3+/2+}$). The EIS data were fitted using a Randles circuit model, indicating that H^+ consumption during ORR altered the interfacial electrostatic landscape, supporting the presence of localized pH elevation and a transition toward a negatively charged surface.[32,33] This phenomenon mirrors trends reported for BOx interfaces in biofuel cells but benefits here from the high surface area, porosity, and hydrophilicity afforded by the walnut shell-derived carbon, which reduce baseline impedance and enhance wettability relative to planar conductive supports.

Capacitive measurements further supported this interfacial restructuring. Analysis of the double-layer capacitance (C_{dl}), derived from non-Faradaic CVs before and after ORR, showed a significant increase—from 0.22 ± 0.03 to 1.3 ± 0.2 mF—only in electrodes bearing both the enzymatic and electrostatic components (Figure 2E, blue curve). In contrast, electrodes lacking either boronic acid moieties or the catalytic enzyme exhibited negligible change in capacitance (black and red curves), demonstrating that both ORR and the Tr^+–BA surface functionalities are prerequisites for dynamic ionic restructuring. These results corroborate earlier studies on stimuli-responsive polymer brushes, yet the present system achieves comparable or superior modulation using a single-layer hybrid interface, fabricated via simpler and more robust chemistries.[8]

Additional CVs at variable scan rates (5–500 mV s^{-1}) confirmed the enhanced capacitive current response post-ORR, with peak current increasing by 340% (Figure 2D, first 30 min), and electron transfer behavior shifting from quasireversible to diffusion-controlled kinetics. This electrochemical transition supports the hypothesis of surface recharging via localized pH shift and is reminiscent of the reversible charge inversion mechanisms observed in polyelectrolyte-modified electrodes, though the present platform demonstrates faster response times and improved operational resilience.[2]

To probe the functionality of the anodic half-cell, the electrochemical behavior of the PQQ-GDH/PDA-modified electrode was assessed in the presence and absence of a competing enzymatic system. Upon addition of 10 mM glucose, the anodic catalytic current increased from 21 ± 4 to 67 ± 9 μA at +0.4 V, indicative of effective glucose oxidation by immobilized PQQ-GDH (**Figure 3**, green trace). When GOx and CAT coimmobilized onto MNPs were introduced and magnetically directed toward the anode (0.3 T), the current was suppressed by 60%, decreasing to 27 ± 4 μA (Figure 3, red trace).

This attenuation is attributed to the preferential glucose consumption by GOx, diverting substrate away from the anode and

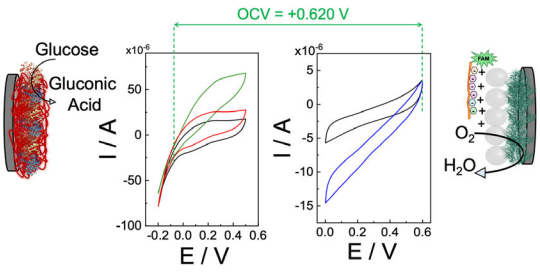

Figure 3. CVs for $(PQQ\text{-}GDH/PDA)_{OPA}/G$ electrode performed in 3 mM HEPES pH 7 + 100 mM Na_2SO_4 (black curve), after the addition of 10 mM D-glucose (green curve) in the presence of a competing enzymatic system (GOx-CAT/MNPs) but without magnetic field, and after the application of a magnetic field of 0.3 T in the presence of a competing enzymatic system (GOx-CAT/MNPs–red curve) at 5 mV s^{-1}; CVs for FAM-DNA/Tr^+-BA^-(1:4)-SiO_2/BOx/C electrode in 3 mM HEPES buffer pH 7 + 100 mM Na_2SO_4 under N_2 purging (black curve) and in open air (blue curve) at 5 mV s^{-1}.

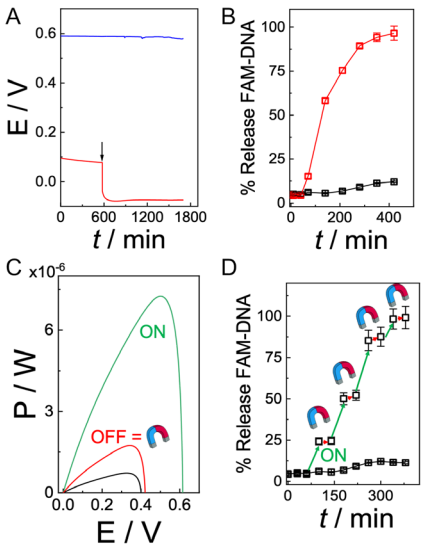

Figure 4. A) OCP curves measured for $(PQQ\text{-}GDH/PDA)_{OPA}/G$ electrode (red curve) in 3 mM HEPES pH 7 + 100 mM Na_2SO_4 (arrow: addition of 10 mM D-glucose) and FAM-DNA/Tr^+-BA^-(1:4)-SiO_2/BOx/C electrode in 3 mM HEPES buffer pH 7 + 100 mM Na_2SO_4 in open air. B) FAM-DNA release curve from $(PQQ\text{-}GDH/PDA)_{OPA}/G$ electrode combined with FAM-DNA/Tr^+-BA^-(1:4)-SiO_2/BOx/C electrode in 3 mM HEPES buffer pH 7 + 100 mM Na_2SO_4 in open air but without the addition of D-glucose (black curve and dots) and after the addition of 10 mM D-glucose (red curve and dots). C) polarization curves measured for $(PQQ\text{-}GDH/PDA)_{OPA}/G$ electrode combined with FAM-DNA/Tr^+-BA^-(1:4)-SiO_2/BOx/C electrode in 3 mM HEPES buffer pH 7 + 100 mM Na_2SO_4 in open air but without the addition of D-glucose (black curve), after the addition of 10 mM D-glucose (green curve) in the presence of a competing enzymatic system (GOx-CAT/MNPs) but without a magnetic field, and after the application of magnetic field of 0.3 T in the presence of a competing enzymatic system (GOx-CAT/MNPs–red curve). D) FAM-DNA release curve from $(PQQ\text{-}GDH/PDA)_{OPA}/G$ electrode combined with FAM-DNA/Tr^+-BA^-(1:4)-SiO_2/BOx/C electrode in 3 mM HEPES buffer pH 7 + 100 mM Na_2SO_4 in open air but without the addition of D-glucose (black curve and dots) and after the addition of 10 mM D-glucose (green curve) in the presence of a competing enzymatic system (GOx-CAT/MNPs) but without a magnetic field, and after the application of magnetic field of 0.3 T in the presence of a competing enzymatic system (GOx-CAT/MNPs—red curve) to simulate ON-OFF system.

effectively gating the electron flow through the system. This type of dynamic enzymatic competition—spatially activated via magnetic fields—represents a novel method for biocatalytic signal regulation not previously employed in electrochemically triggered DNA release systems.[34]

The coupling of the PQQ-GDH anode and the BOx-functionalized cathode enabled real-time control over DNA release through localized pH modulation. Upon glucose addition, the local pH at the cathode increased from pH 7 to pH 10.2, as protons were consumed during enzymatic oxygen reduction (comparison with data previously reported). The resulting shift in surface charge led to the release of electrostatically bound FAM-DNA. Concurrently, the open circuit potential (OCP) of the anode decreased from $+94 \pm 4$ to -59 ± 7 mV vs. Ag/AgCl (**Figure 4**A), consistent with increased cathodic activity. Fluorescence analysis indicated a cumulative DNA release of 97% over 400 min, corresponding to 22 ± 4 nmol cm^{-2} (Figure 4B, calculated based calibration curve reported in Figure S2, supporting information), values comparable to or exceeding those achieved in potentiostatically triggered release systems, while offering self-powered and reversible control.

The use of GOx–CAT/MNPs also enabled externally modulated "OFF" states. In the absence of a magnetic field, the MNPs remained dispersed and uninvolved in catalysis, allowing normal DNA release. Upon magnetic activation, the GOx–CAT/MNPs accumulated at the anode, diverting glucose oxidation away from PQQ-GDH and reducing cathodic ORR activity. This inhibition decreased FAM-DNA release to 1% (Figure 4D) and corresponded to a reduction in anodic current from 67 ± 9 to 27 ± 4 μA (Figure 4C). Indeed, power output measurements under operating conditions revealed a peak output of 7.2 ± 0.9 μW, demonstrating that the system functions as a self-sufficient biosignal processor without requiring external biasing. Compared to traditional DNA release strategies relying on externally imposed potentials or light sources, this configuration allows autonomous actuation using endogenous substrates such as glucose—an important advance for bioelectronic systems in wearable or implantable formats.[31]

Unlike photochemical or chemical gating strategies, magnetic field-based actuation offers noninvasive, reversible, and spatiotemporally precise control, with minimal risk of photodamage or chemical contamination.[31]

Fluorescence microscopy confirmed robust system performance across multiple actuation cycles. After the first ON-state triggering, a 25% decrease in surface fluorescence was observed after the first ON-OFF cycle, up to 94% after the third ON-OFF cycle indicating substantial DNA release. Subsequent ON–OFF cycles resulted in consistent and repeatable fluorescence drops (**Figure 5**A–D), with negligible signal decay. This level of stability surpasses that of earlier DNA release systems using polyelectrolyte or thiol-based assemblies, which typically suffer from partial fouling, irreversible bond cleavage, or interface degradation after a few cycles.[35,36]

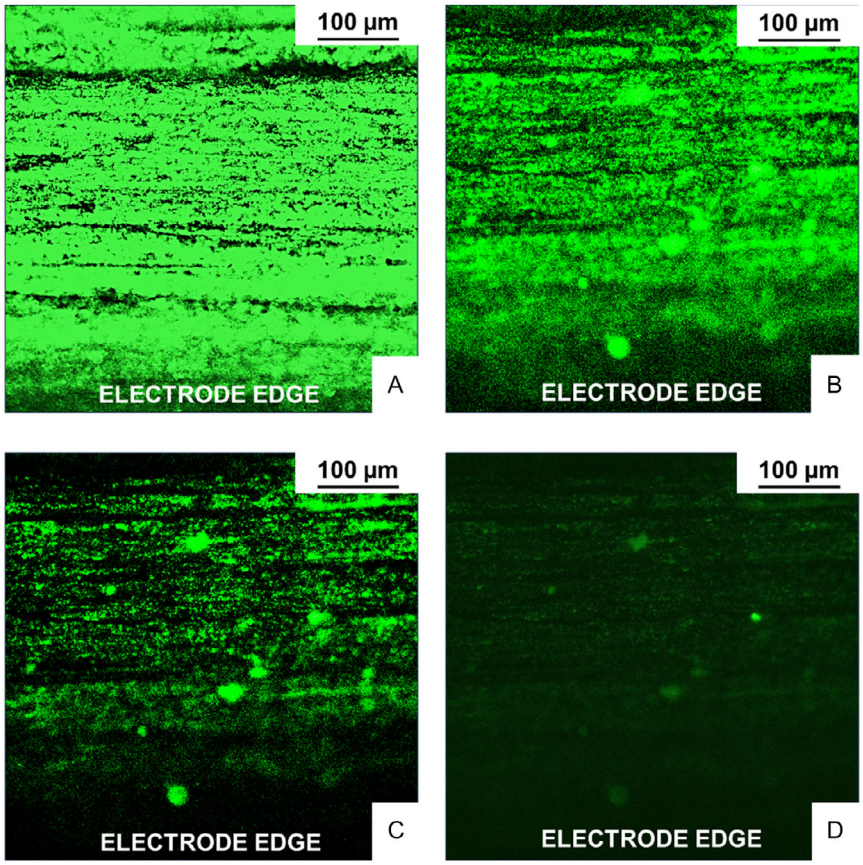

Figure 5. Fluorescent microscopy image for FAM-DNA/Tr^{+}-BA^{-}(1:4)-SiO_2/BOx/C electrode at A) t = 0 min, B) after I ON-OFF cycle, C) after II ON-OFF cycle, and D) after III ON-OFF cycle.

Table 1 presents a comparative analysis against conventional DNA release strategies. Traditional approaches—spanning passive diffusion, pH-responsiveness, enzymatic degradation, and thermally induced desorption—typically lack real-time external control, exhibit limited spatial resolution, and are often incompatible with autonomous or bioelectronic integration. In contrast, the electrochemically actuated platform introduced here offers fully reversible, spatiotemporally precise DNA release, operating near-zero bias through a self-sustained enzymatic oxygen reduction cascade. While the release kinetics (≈400 min) remain longer than those of thermally triggered systems, they are intrinsically governed by the sluggish kinetics of the ORR at neutral pH—a well-documented limitation in electrochemical systems operating under physiological conditions.

Importantly, this latency is addressable through surface charge engineering of the nanoparticle interface or substitution with faster redox chemistries, both of which are under active investigation. Beyond kinetic metrics, the present work delineates a previously unexplored paradigm: an ingestible, magnetically switchable, enzymatically powered electrochemical platform capable of autonomous drug release modulation. The use of fluorescently labelled DNA as a model payload validates the system's functionality, while its modular design supports translation to therapeutic biomacromolecules such as insulin. As the first

Table 1. Comparative analysis of the proposed electrochemical DNA release platform with conventional release strategies.

Release strategy	Trigger type	vTemporal control	Spatial control	On-demand actuation	Biocompatibility	Integration potential	Typical release time
Electrochemical (this work)	Electrical/redox trigger	High	High	Yes	High (ORR-based)	High (ingestible electronics)	Minutes to hours
Passive diffusion	No external trigger	Low	None	No	High	Low	Hours to days
pH-responsive systems	Local pH variation	Moderate	Moderate	Partial	Variable	Moderate	Minutes to hours
Enzymatic degradation	Enzyme–substrate interaction	Low	Low	No	High	Low	Hours
Thermo-responsive systems	Temperature increase	Moderate	Low	Partial	Limited (in vivo)	Moderate	Minutes

demonstration of a self-regulated, sense–act–treat device built entirely from sustainable materials, this architecture represents a foundational advance in the field of intelligent bioelectronic therapeutics and responsive drug delivery systems.[37,38]

3. Conclusions

In this study, we developed a magnetically switchable bioelectronic interface capable of real-time, reversible DNA release, driven entirely by a self-sustained enzymatic system integrated onto biomass-derived carbon electrodes. The platform couples glucose oxidation at a PQQ–GDH/PDA-modified anode with oxygen reduction at a bilirubin oxidase-based cathode to locally modulate pH and trigger the release of boronate-bound 5(6)-carboxyfluorescein-labeled DNA (FAM–DNA). Reversible DNA capture and release were achieved using silica nanoparticles co-functionalized with trigonelline and boronic acid, enabling noncovalent, electrostatically controlled interactions modulated by enzymatically driven pH shifts. Electrochemical measurements revealed a catalytic onset potential of $+0.576 \pm 0.003$ V vs. Ag/AgCl and a maximum current of -8.2 ± 0.4 μA under aerobic conditions. DNA release efficiency reached 97% within 400 min, corresponding to 22 ± 4 nmol cm^{-2} surface coverage. Remote actuation was enabled by a magnetically addressable enzymatic gate comprising GOx–CAT-modified MNPs, which suppressed the anodic reaction and reduced current output by 60% under "OFF" conditions. The system maintained high operational stability across four switching cycles with negligible signal loss. Notably, all enzymatic and electrochemical processes occurred near 0 V vs. Ag/AgCl, ensuring compatibility with physiological environments and minimizing the risk of redox-induced degradation. This work establishes a proof-of-concept for integrating renewable materials, self-powered catalysis, and external-field logic gating into programmable platforms for intelligent nucleic acid delivery. The proposed architecture offers a scalable and sustainable route toward next-generation autonomous diagnostic and therapeutic devices.

4. Experimental Section

Chemicals and Reagents: All chemicals were of analytical grade and used without additional purification. Pyrroloquinoline quinone-dependent glucose dehydrogenase (PQQ-GDH, EC 1.1.5.2) from *Acinetobacter calcoaceticus* and bilirubin oxidase (BOx, EC 1.3.3.5) from *Myrothecium verrucaria* were supplied by Toyobo Co., Ltd. and Amano Enzyme Inc., respectively. Glucose oxidase (GOx, EC 1.1.3.4) and catalase (CAT, EC 1.11.1.6) derived from *Aspergillus niger* were obtained from Sigma-Aldrich. Trigonelline (1-methylpyridinium-3-carboxylate), 4-carboxyphenylboronic acid (BA), dopamine hydrochloride, EDC (N-(3-dimethylaminopropyl)-N′-ethylcarbodiimide), NHS (N-hydroxysuccinimide), MES buffer, and glutaraldehyde solution (25% w/w) were purchased from Merck or Sigma-Aldrich. Amine-functionalized MNPs (Fe_3O_4, ≈100 nm diameter) were provided by Chemicell GmbH. Silica nanoparticles (200 nm diameter) were sourced from Fiber Optic Center Inc. Custom-synthesized FAM-labeled single-stranded DNA (5′-FAM-TGC AGA CGT TGA AGG ATC CTC-3′) was obtained from Integrated DNA Technologies (IDT). All buffer salts, including HEPES, PBS, KCl, and Na_2SO_4, were acquired from Merck or Thermo Fisher Scientific.

Synthesis of Walnut Shell-Derived Carbon Electrodes: Dried walnut shells were ground, cleaned, and subjected to pyrolysis under inert atmosphere (N_2 flow, 900 °C, 2 h) to produce conductive carbon materials. The resulting product was pressed into flexible sheets or compacted into disk electrodes (geometric area: 0.07 cm^2), followed by mechanical polishing and sonication in ethanol and deionized water.[39] The pyrolyzed carbon was selected for its high surface area and structural porosity, features advantageous for biomolecule immobilization and charge transport.

Assembly of the Cathodic Interface: The carbon working electrodes were first functionalized with polyethylenimine (PEI, 1 mg mL^{-1}) to introduce surface amines. BOx (1 mg mL^{-1} in PBS) was then covalently tethered to the PEI layer using 2.5% glutaraldehyde as a crosslinking agent.[8] In parallel, silica nanoparticles were functionalized through silanization with (3-Aminopropyl)triethoxysilane (APTES) and sequentially conjugated with trigonelline and 4-carboxyphenylboronic acid in a 1:4 molar ratio via EDC/NHS chemistry in MES buffer (pH 6.0). The resulting bifunctional SiO_2-NPs were deposited dropwise onto the BOx-modified carbon electrodes and allowed to dry at ambient temperature. To immobilize FAM-labeled DNA, the functionalized electrodes were immersed in a 1 μM FAM-labeled DNA solution prepared in 10 mM HEPES buffer (pH 7.0, 100 mM KCl) for 30 min and then gently rinsed to remove unbound molecules.

Fabrication of the Bioanode and Enzymatic Gate System: For anodic biofunctionalization, a one-step PDA deposition protocol was used. Carbon electrodes were immersed in 2 mg mL^{-1} dopamine hydrochloride solution in Tris-HCl buffer (10 mM, pH 8.5) for 2 h to allow in situ polymerization.[40] After rinsing, PQQ-GDH (1 mg mL^{-1} in PBS) was adsorbed onto the PDA surface by incubation for 30 min. For the competing enzymatic system, GOx and CAT were coimmobilized on amine-functionalized MNPs via glutaraldehyde crosslinking.[41] After coupling, the particles were washed with PBS and resuspended at a final concentration of 50 μg mL^{-1} for use in magnetic field modulation experiments.

Electrochemical and Fluorescence Characterization: Electrochemical experiments were carried out using PalmSens4 electrochemical workstation equipped with the PSTrace 5.6v software in a three-electrode setup comprising the modified carbon electrode (working), Ag/AgCl (3 M KCl, reference), and a Pt wire (counter). All measurements were performed in HEPES buffer (10 mM, pH 7.0) containing 100 mM Na_2SO_4 as the supporting electrolyte. CV and OCP were recorded at room temperature. EIS was conducted using 1 mM $[Fe(CN)_6]^{3-/4-}$ in the same buffer, scanning from 100 kHz to 0.01 Hz with an amplitude of 10 mV. Similarly, EIS experiments were performed also in 1 mM $[Ru(NH_3)_6]^{3+/2+}$ in HEPES buffer (10 mM, pH 7.0) containing 100 mM Na_2SO_4. Fluorescence measurements were performed using a Tecan Infinite M200 microplate reader (excitation/emission: 495/520 nm). Confocal fluorescence microscopy was conducted with a Leica TCS SP8 system to visualize DNA adsorption and release on the electrode surface.

Protocol for Magnetically Controlled DNA Release: To initiate the "ON" state, 10 mM D-glucose was added to the cell under ambient conditions to activate anodic PQQ-GDH catalysis, enabling electron flow to the cathode and promoting oxygen reduction. Proton consumption at the cathode led to a localized pH rise, triggering electrostatic desorption of FAM-DNA. To achieve the "OFF" state, GOx–CAT-loaded MNPs were added to the system and localized to the anodic region using an external neodymium magnet (0.3 T). This diverted glucose oxidation away from PQQ-GDH, halting electron transfer and suppressing DNA release. Cycling between ON and OFF conditions was achieved by alternately adding glucose and applying the magnetic field.

Supporting Information

Supporting Information is available from the Wiley Online Library or from the author.

Acknowledgements

The following funding agencies are acknowledged: NoOne—a binary sensor with a single-molecule digit to discriminate biofluids enclosing zero or at least one biomarker, ERC Stg2021, GA:101040383; Centro di

Innovazione in Single-Molecule Digital Assay—"Digital Assay" from Regione Puglia DGR N. 218 of 21/02/2022; Italian network of excellence for advanced diagnosis (INNOVA), Ministero della Salute -code PNC-E3-2022-23683266 PNC-HLS-DA, CUP: C43C22001630001; Complementary National Plan PNC-I.1 "Research initiatives for innovative technologies and pathways in the health and welfare sector" D.D. 931 of 06/06/2022, DARE—DigitAl lifelong pRevEntion initiative, code PNC0000002. This work was partially supported by the European Union under the Italian National Recovery and Resilience Plan (NRRP) of NextGenerationEU, the partnership on "Telecommunications of the Future" (PE00000001 - program "RESTART," Structural Project DREAMS), and CSGI (Centre for Colloid and Surface Science).

Open access publishing facilitated by Universita degli Studi di Bari Aldo Moro, as part of the Wiley - CRUI-CARE agreement.

Conflict of Interest

The authors declare no conflict of interest.

Author Contributions

Paolo Bollella: conceptualization (lead); funding acquisition (supporting); methodology (lead); supervision (equal); visualization (lead); writing—original draft (lead). **Blanca Cassano**: data curation (supporting); formal analysis (supporting); investigation (equal). **Verdiana Marchianò**: data curation (equal); formal analysis (equal); investigation (equal). **Angelo Tricase**: data curation (supporting); formal analysis (supporting); investigation (equal); methodology (supporting); visualization (supporting). **Eleonora Macchia**: conceptualization (supporting); funding acquisition (lead); supervision (equal); validation (equal); writing—review and editing (equal). **Luisa Torsi**: conceptualization (lead); funding acquisition (lead); supervision (lead); writing—original draft (lead); writing—review and editing (equal).

Data Availability Statement

The data that support the findings of this study are available from the corresponding author upon reasonable request.

Keywords

DNA releases, enzyme based electrodes, local pH changes, ON-OFF bioelectrochemical systems, oxygen reduction reactions

Received: May 19, 2025
Revised: July 27, 2025
Published online:

[1] E. Katz, *Enzyme-Based Computing Systems*, Wiley-VCH Verlag GmbH & Co, Weinheim, Germany **2019**.
[2] P. Bollella, A. Melman, E. Katz, *ChemElectroChem* **2020**, *7*, 3386.
[3] G. K. Kashani, S. M. Naghib, S. Soleymani, M. R. Mozafari, *Int. J. Biol. Macromol.* **2024**, *268*, 131694.
[4] M. E. Caldorera-Moore, W. B. Liechty, N. A. Peppas, *Acc. Chem. Res.* **2011**, *44*, 1061.
[5] A. A. Tregubov, P. I. Nikitin, M. P. Nikitin, *Chem. Rev.* **2018**, *118*, 10294.
[6] Y. Zhang, J. Tu, D. Wang, H. Zhu, S. K. Maity, X. Qu, B. Bogaert, H. Pei, H. Zhang, et al., *Adv. Mater.* **2018**, *30*, 1703658.
[7] H. Lv, N. Xie, M. Li, M. Dong, C. Sun, Q. Zhang, L. Zhao, J. Li, X. Zuo, H. Chen, F. Wang, C. Fan, et al., *Nature* **2023**, *622*, 202.
[8] M. Masi, P. Bollella, E. Katz, *Electroanalysis* **2020**, *32*, 95.
[9] M. Masi, P. Bollella, E. Katz. *ACS Appl. Mater. Interfaces* **2019**, *11*, 47625–47634.
[10] D. M. Roquero, P. Bollella, A. Melman, E. Katz, *ACS Appl. Bio Mater.* **2020**, *3*, 3741.
[11] S. Mailloux, J. Halámek, E. Katz, *Analyst* **2014**, *139*, 982.
[12] Y. Wang, D. S. Kohane, *Nat. Rev. Mater.* **2017**, *2*, 1.
[13] E. Katz, J. M. Pingarrón, S. Mailloux, N. Guz, M. Gamella, G. Melman, A. Melman, et al., *J. Phys. Chem. Lett.* **2015**, *6*, 1340.
[14] E. Katz, In *Bioelectrochemistry*, (Ed: S. Cosnier), Walter de Gruyter GmbH, Berlin, Germany **2019**, pp. 143–166.
[15] R. Badenhorst, O. Smutok, E. Katz, *ChemElectroChem* **2022**, *9*, e202200897.
[16] J.-M. Pernaut, J. R. Reynolds, *J. Phys. Chem. B* **2000**, *104*, 4080.
[17] D. Svirskis, J. Travas-Sejdic, A. Rodgers, S. Garg, *J. Controlled Release* **2010**, *146*, 6.
[18] M. Bellare, V. K. Kadambar, P. Bollella, E. Katz, A. Melman, *Chem. Commun.* **2019**, *55*, 7856.
[19] D. M. Roquero, P. Bollella, O. Smutok, E. Katz, A. Melman, *Mater. Today Chem.* **2021**, *21*, 100514.
[20] D. Massana Roquero, P. Bollella, E. Katz, A. Melman, *ACS Appl. Polym. Mater.* **2021**, *3*, 1499.
[21] S. D. Minteer, B. Y. Liaw, M. J. Cooney, *Curr. Opin. Biotechnol.* **2007**, *18*, 228.
[22] E. Katz, P. Bollella, *Isr. J. Chem.* **2021**, *61*, 68.
[23] M. Grattieri, S. D. Minteer, *ACS Sens.* **2018**, *3*, 44.
[24] P. Bollella, G. Fusco, D. Stevar, L. Gorton, R. Ludwig, S. Ma, H. Boer, A. Koivula, C. Tortolini, G. Favero, R. Antiochia, F. Mazzei, et al., *Sens. Actuators B Chem.* **2018**, *256*, 921.
[25] P. Bollella, *Anal. Chim. Acta* **2022**, *1234*, 340517.
[26] F. Torricelli, I. Alessandri, E. Macchia, I. Vassalini, M. Maddaloni, L. Torsi, et al., *Adv. Mater. Technol.* **2022**, *7*, 2100445.
[27] V. K. Kadambar, M. Bellare, P. Bollella, E. Katz, A. Melman, *Chem. Commun.* **2020**, *56*, 13800.
[28] C. Santoro, P. Bollella, B. Erable, P. Atanassov, D. Pant, *Nat. Catal.* **2022**, *5*, 473.
[29] A. Tricase, B. Alhenaki, V. Marchianò, L. Torsi, R. Gupta, P. Bollella, et al., *Nanoscale Adv.* **2024**, *6*, 516.
[30] A. Tricase, M. Muhyuddin, B. Erable, P. Atanassov, D. Pant, C. Santoro, P. Bollella, et al., *J. Power Sources* **2025**, *646*, 237267.
[31] A. Roquia, A. Khalfan Hamed Alhashmi, B. Hamed Abdullah Alhasmi, *Fuller. Nanotub. Carbon Nanostruct.* **2021**, *29*, 860.
[32] Y. H. Ding, M. Floren, W. Tan, *Biosurf. Biotribol.* **2016**, *2*, 121.
[33] J. Zhou, T. K. Tam, M. Pita, M. Ornatska, S. Minko, E. Katz, et al., *ACS Appl. Mater. Interfaces* **2009**, *1*, 144.
[34] E. Katz, *Biomolecular information processing: from logic systems to smart sensors and actuators*, John Wiley & Sons **2013**.
[35] P. Bollella, A. Melman, E. Katz, *ChemElectroChem* **2021**, *8*, 3923.
[36] M. C. Monteiro, M. T. Koper, *Curr. Opin. Electrochem.* **2020**, *25*, 100649.
[37] P. Bollella, S. Edwardraja, Z. Guo, K. Alexandrov, E. Katz, *Chem. Commun.* **2020**, *56*, 9206.
[38] K. Wang, K. Amin, Z. An, Z. Cai, H. Chen, H. Chen, Y. Dong, X. Feng, W. Fu, J. Gu, Y. Han, D. Hu, R. Hu, D. Huang, F. Huang, F. Huang, Y. Huang, J. Jin, X. Jin, Q. Li, T. Li, Z. Li, Z. Li, J. Liu, J. Liu, S. Liu, H. Peng, A. Qin, X. Qing, Y. Shen, et al., *Mater. Chem. Front.* **2020**, *4*, 1803.
[39] S. Shakibania, M. J. P. Biggs, K. Krukiewicz, *Adv. Mater. Interfaces* **2024**, *12*, 2400774.
[40] M. Privman, T. K. Tam, V. Bocharova, J. Halámek, J. Wang, E. Katz, et al., *ACS Appl. Mater. Interfaces* **2011**, *3*, 1620.
[41] R. A. Siegel, *J. Controlled Release* **2014**, *190*, 337.

